photonics

MDPI

Communication

Effect of Beam-Steering Angle, Operation Wavelength and Mean Inter-Element Distance on the Side-Lobe Levels of Integrated Optical Phased Arrays under Beam-Steering Operation

Ivan Aldaya [1,2,*], Bruna Dias Pires de Souza [1], Rafael Abrantes Penchel [1,2], Julian Leonel Pita [3], Mirian Paula dos Santos [1,2], José Augusto de Oliveira [1,2] and Marcelo Luis Francisco Abbade [1]

[1] School of Engineering of São João da Boa Vista, São Paulo State University (Unesp), São João da Boa Vista 13876-750, Brazil; bruna.dias@unesp.br (B.D.P.d.S.); rafael.penchel@unesp.br (R.A.P.); mirian.santos@unesp.br (M.P.d.S.); jose.a.oliveira@unesp.br (J.A.d.O.); marcelo.abbade@unesp.br (M.L.F.A.)
[2] Center for Advanced and Sustainable Technologies, São Paulo State University (Unesp), São João da Boa Vista 13876-750, Brazil
[3] Telecommunications and Microelectronics Integration Laboratory, École de Technologie Supérieure, Montreal, QC H3C 1K3, Canada; jlpitar@unal.edu.co
* Correspondence: ivan.aldaya@unesp.br; Tel.: +55-(19)-3638-2400

Abstract: Integrated optical phased arrays (OPAs) play an important role in a broad range of applications. Fabrication constraints, however, pose a limit to the minimum inter-element separation that further results in high-intensity side lobes. The intensity of these secondary lobes can be reduced by arranging the antenna elements with non-uniform separation distance, which has been addressed by different methods. In this paper we employ one of the already proven optimization algorithms, i.e., differential evolution, to optimize the element positions of linear arrays with different configurations operating under beam-steering operation and considering a minimum inter-element distance. These optimizations allowed us to derive some design guidelines that can assist in reducing the side-lobe level (SLL) of integrated linear OPAs. In particular, we found that it is necessary to optimize the positions for the broadest beam-steering angle and the shortest operation wavelength. Additionally, optimizations of different configurations reveal that, when imposing a minimum inter-element distance, there is an optimum mean distance that minimizes the SLL of the array.

Keywords: optical phased arrays; side-lobe level; differential evolution

Citation: Aldaya, I.; Pires de Souza, B.D.; Penchel, R.A.; Pita, J.L.; dos Santos, M.P.; de Oliveira, J.A.; Abbade, M.L.F. Effect of Beam-Steering Angle, Operation Wavelength and Mean Inter-Element Distance on the Side-Lobe Levels of Integrated Optical Phased Arrays under Beam-Steering Operation. *Photonics* **2023**, *10*, 1300. https://doi.org/10.3390/photonics10121300

Received: 17 July 2023
Revised: 8 August 2023
Accepted: 14 August 2023
Published: 24 November 2023

1. Introduction

Photonic antennas have attracted increasing interest in recent years due to their critical role in areas as diverse as spectroscopy [1], optical communications [2] and light detection and ranging (LIDAR) [3]. The first developed antennas operating in the range of optical frequencies exploited the plasmonic resonance of metallic surfaces [4]. Such antennas can present small dimensions but they typically show low efficiency and pose serious feeding challenges. In order to overcome these issues, all-dielectric photonic antennas were proposed [5]. In addition to high efficiency, all-dielectric antennas can be integrated not only with the feeding waveguide but also with other integrated devices such as phase-shifters and modulators, as well as with the associated control and signal processing electronics [6]. However, these advantages can only be achieved at the expense of a significant size increase. This issue is especially critical in the design and implementation of optical phased arrays (OPAs), where multiple coherently-fed elements are used to allow the tailoring of the radiation pattern and its dynamical control. OPAs are particularly useful in applications where some kind of scanning or alignment is needed, for instance in re-configurable free-space optical cross-connects [7] and in electrically steerable LIDARs [8].

OPAs can be roughly classified into linear and planar arrays, each of them having its applications and design particularities. In particular, linear arrays typically present lower cost and smaller occupation area and, therefore, are preferable in applications where the beam steering should be performed in mainly one direction. Additionally, linear phase arrays can be designed to radiate either in the direction of the substrate plane or in a direction not contained in this plane as can be seen in Figure 1: (a) in-plane linear OPA and (b) out-of-plane linear OPA.

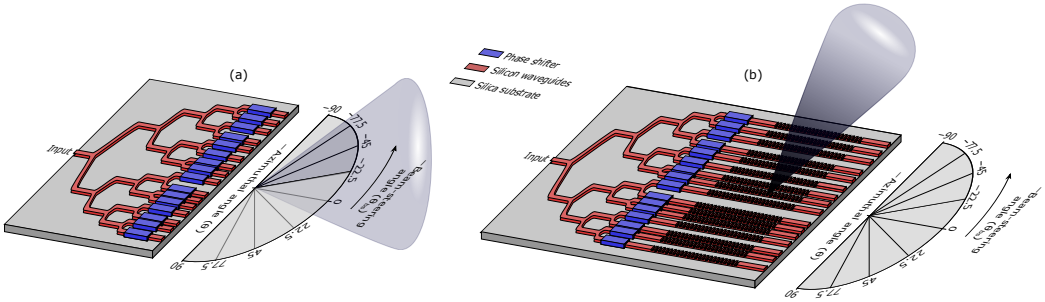

Figure 1. Examples of integrated linear OPAs: (**a**) in-plane emission and (**b**) out-of-plane emission.

The large antenna size of all-silicon antennas then limits the minimum separation in OPAs. In addition, the minimum inter-element separation is further increased when the OPA is implemented on integrated photonics, e.g., silicon on insulator, where the antenna elements are typically built in the same layer as the feeding network and phase and amplitude control elements [9]. In this case, if antenna elements are uniformly distributed, that is, if the separation between elements is the same, the radiated fields do not interfere constructively only in the desired direction but also in other directions, leading to high-intensity lobes that are denominated grating lobes. The intensity and number of these grating lobes depend on the inter-element separation and the beam-steering angle (the angle in which the main lobe is directed) and they should be minimized, as they can cause crosstalk, security faults and degrade the signal-to-noise ratio [10,11]. In order to minimize the intensity of these lobes, in [12], the authors employed an array of waveguides with tailored widths specially designed to minimize the coupling; thus, allowing the reduction of inter-element separation. The most adopted solution, however, is to arrange the elements in a non-uniform configuration; that is, with different inter-element separations.

Arranging the elements non-uniformly turns the antenna design into a combinatory mathematical optimization problem that has been extensively studied in RF applications, where sparse arrays are attractive because of their good trade-off between cost and gain and the reduced near-field coupling between elements. Thus, a plethora of optimization algorithms has been proposed, both deterministic and heuristic. Among the employed deterministic algorithms, we can mention the discretization of the radiation integral [13,14], tapering using geometrical progression [10] and the optimization via cyclic difference sets [15]. Nevertheless, heuristic methods have shown better performance and are more widely adopted. For instance, in [16], simulated annealing is proposed, whereas in [17] and in [18], particle swarm is employed. Evolutionary computing has also been extensively studied. In [11,19–24], the optimization is performed using genetic algorithms and in [25–27], different configurations of differential evolution are employed. However, most of these works are focused on optimizing the position of the elements without analyzing the effect of structural (number of elements and mean and minimum inter-element distances) and operational parameters (operating wavelength and beam-steering direction). For instance, only [10,11,19,20,24] consider emission in out-of-broadside angles and only [11,14,16,19,20,25,27] include a minimum inter-element separation as an optimization constrain. This means that just [11] considers simultaneously beam-steering operation and minimum inter-element spacing. However, the interdependence among the different structural and operational parameters is still not clear.

In this paper, we do not intend to propose or compare optimization algorithms to find the optimum antenna position, but to analyze the effect of the beam-steering angle and the minimum separation distance on the side-lobe level (SLL) in terms of the number of elements and the average inter-element separation distance, which allows us to derive some design guidelines. In particular, we show that it is enough to optimize the positions of elements for the maximum steering angle to ensure that the SLL is lower for the complete beam-steering range. A similar behavior is observed in relation to the operating wavelength. Since the SLL reduces as the operation wavelength increases, it is necessary to optimize the positions for the shortest wavelength of the operation band. In addition, the optimizations for different array configurations reveal that when setting a minimum inter-element distance, there is an optimum average separation that minimizes the SLL of the OPA. Finally, we discuss the possibility of adopting sectorized antennas to reduce the SLL of the complete OPA, as this reduces the maximum steering angle of each sector.

2. Optimization of Element Positions

Assuming that the mean inter-element distance is fixed and that the separation cannot be smaller than d_{min}, the search for optimum positions of N elements has $N-1$ degrees of freedom. The problem can be mathematically formulated as:

$$\begin{aligned} &\text{argmin}_{X=\{x_k\}} SLL(X, \theta_{BS}) \\ &\text{subject to:} \\ &\quad \text{(i) } d_k = x_k - x_{k-1} \geq d_{min} \text{ with } k = 2, \ldots, N \\ &\quad \text{(ii) } \sum_{k=2}^{N} d_k = L, \end{aligned} \tag{1}$$

where $SLL(\theta_{BS}, X)$ is the SLL of the array with elements located at positions x_k and the main lobe is directed towards θ_{BS}. If the coupling between the antenna elements is weak, the field radiated by an array of N identical elements located at positions z_n along the z axis can be approximated by:

$$\vec{E}(\theta, \phi, X) = \sum_{i=1}^{N} \vec{E}_{el}(\theta, \phi) \exp[j(kz_i \cos\theta + \phi_i)], \tag{2}$$

where $\vec{E}_{el}(\theta, \phi)$ is the electric field radiated by the radiating element centered at the origin, k is the wave number, θ is the azimuthal angle and ϕ_n is the phase of the feeding of the n-th element. The total radiated field can be alternatively expressed as the product of the field of the radiating elements and a term that accounts for the element positions and their phases, denominated the array factor (AF):

$$\vec{E}(\theta, \phi, X) = \vec{E}_{el}(\theta, \phi) \cdot AF(\theta, X, \theta_{\text{BS}}). \tag{3}$$

For a linear array, the AF only depends on θ, the set of element positions X and the beam-steering angle that sets the phases ϕ_i. Thus, considering an array of low-directivity radiating elements, the maximum value of the norm of the AF equals the number of elements; because, in this direction, all of the elements interfere constructively. Regarding the SLL, it can be obtained from the AF as:

$$SLL(X, \theta_{\text{BS}}) = \left| \frac{AF(\theta_{\text{BS}}, X, \theta_{\text{BS}})}{AF(\theta_{\text{sec}}, X, \theta_{\text{BS}})} \right|. \tag{4}$$

$AF(\theta_{\text{BS}}, X, \theta_{\text{BS}})$ and $AF(\theta_{\text{sec}}, X, \theta_{\text{BS}})$ are the values of the array factor at the desired radiation direction and at the direction of the strongest side lobe [28]. The minimization has a twofold constraint: on the one hand, the separation between the adjacent elements $d_k = x_k - x_{k-1}$ has to be larger than d_{min}. On the other hand, the total length of the array is set to L, which

can be alternatively written in terms of the mean distance $\bar{d}$ as $L = (N-1) \cdot \bar{d}$. The adopted angle criteria and the nomenclature are shown in Figure 2, alongside a block diagram of a non-uniformly distributed array antenna and a graphical representation of phases of the feeding.

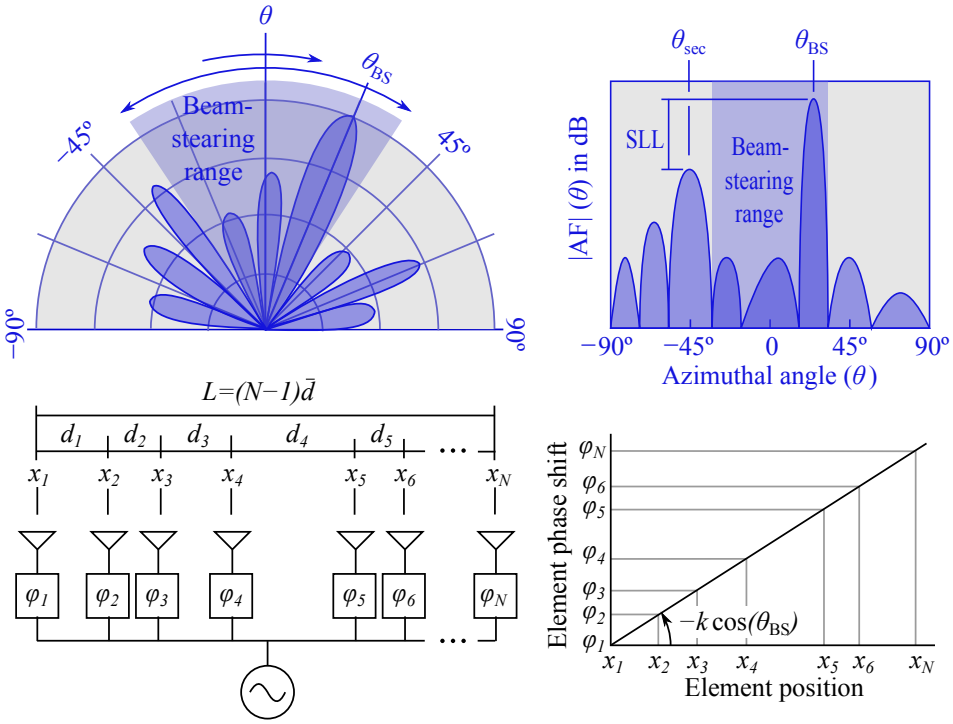

Figure 2. Schematic of the linear sparse antenna alongside an illustrative polar and Cartesian representation of the AF indicating the employed nomenclature. A graphical representation of the relation between the phase of the feeding and the element positions is also shown.

Even for a relatively low number of elements, the SLL minimization cannot be addressed by brute force. In order to find sub-optimal but acceptable solutions, different heuristic methods have been proposed. Among the different algorithms used to optimize the element positions in non-uniform sparse linear arrays [26], differential evolution (DE) has demonstrated a good trade-off between complexity and performance, which has led many authors to use this heuristic algorithm [29–31]. DE emulates the natural evolution of species by improving the quality of successive generations [32]. Within each iteration, DE selects the solutions (individuals) out of a set of tentative solutions that present the best performance in terms of the metric to be optimized, denominated as cost function. These individuals are combined (crossed-over) and randomly modified (mutated) to generate a new improved generation of solutions. Once the best tentative solution attains an acceptable value or no further improvement is achieved, the algorithm execution stops.

The results presented in Section 3 were obtained using a DE algorithm with a crossover probability of 0.1 and a scaling factor ranging from 0.2 to 0.8 [33]. The constraints in (1) were introduced by means of a normalization of the newly generated solutions. To dimension the size of the population and the number of iterations, we conveyed initial optimizations showing that an acceptable trade-off between complexity and performance is achieved by employing a population size of 40 individuals, 100 random initial populations and a number of iterations that depends on the number of antenna elements: 500 for 4 elements, 1000 for 8 elements and 3000 for 16 elements. The convergence of the algorithm can be observed in Figure 3, where each trace corresponds to the metric (in our case, the SLL) of the best individual of the evolution of an independent initial population. Figure 3a is for 4-element arrays whereas Figure 3b and Figure 3c are for 8 and 16 elements respectively. Looking at the traces, it can be concluded that some initial populations lead to

poor solutions, so by choosing independent random populations, the sensitivity to initial conditions is mitigated. Comparing the traces for different numbers of antenna elements, the populations of arrays with a lower number of elements converge more rapidly. For a larger number of elements, DE requires more iterations and the final configurations present a higher variance. Both observations can be justified by the higher dimension of the solution space of higher element solutions.

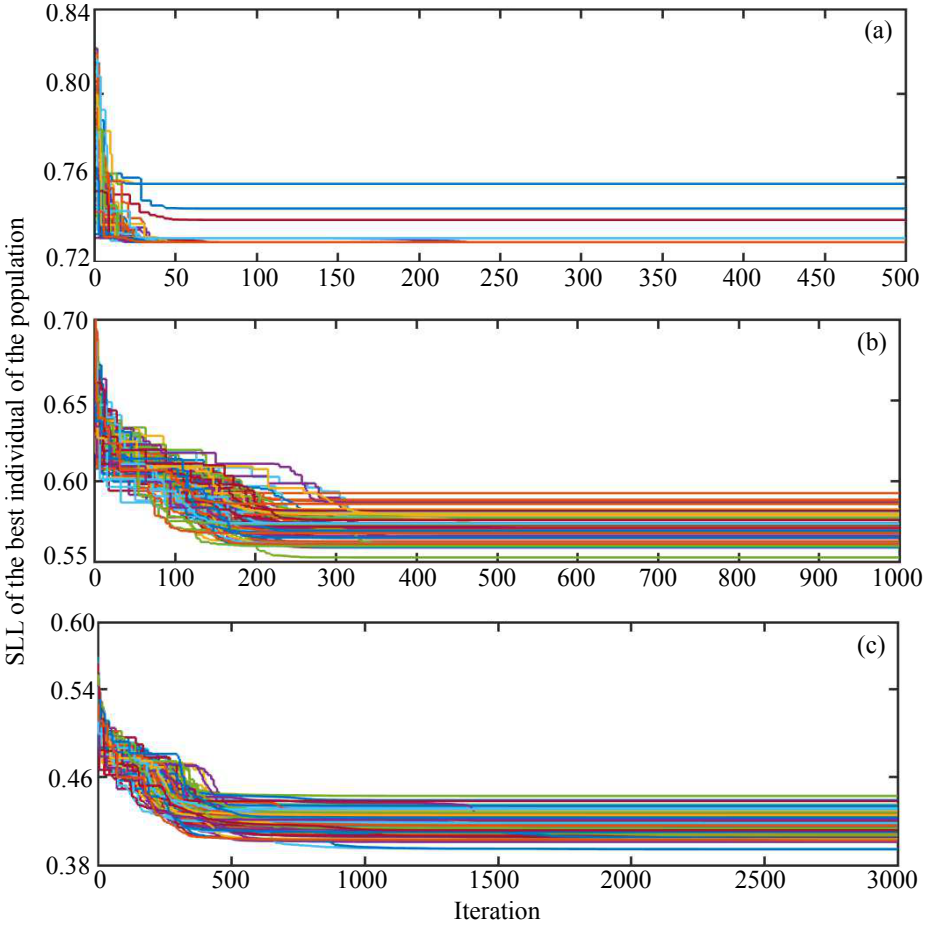

Figure 3. Evolution of the SLL of the best individual in terms of the iteration for (**a**) 4-element, (**b**) 8-element and (**c**) 16-element antenna. In each subfigure, the different traces correspond to independent random initial populations.

3. Results

The SLL is influenced by a great number of parameters, of which the most important are the beam-steering angle, the operation wavelength, the inter-element distance and the number of elements. In order to analyze their effect and interplay, we divide this section into three subsections.

3.1. Effect of Beam-Steering Angle and Operation Wavelength on the Side-Lobe Level

First, we analyzed the effect of beam steering and the target steering range on the SLL value. In Figure 4a we show the positions of 8-element arrays optimized for three different steering ranges: 0°, 22.5° and 45°, setting the minimum distance between elements to 2λ and a mean separation of 6λ. It can be noted that the element positions depend on the target steering angle. The SLL of the arrays designed for the three steering ranges are shown in Figure 4b. As can be observed, at 0°, the configuration optimized for a range of 0° (no beam steering) outperforms arrays optimized for steering ranges of 22.5° and 45°. However, for beam-steering angles between 0° and 22.5°, the array optimized for a range of 22.5° presents the best performance. Similar behavior can be observed for the

beam-steering angles up to 45° when beam-steering angles between 22.5° and 45° are considered. It is important to note that, as envisaged, the SLL worsens as the beam-steering angle is increased. Thus, optimizing for a whole range is equivalent to optimizing for the maximum beam steering; that is, for the extreme value of the target steering range. In fact, the SLL presents a monotonically increasing stair-case shape, which can be understood by observing the evolution of the radiation diagram as the beam-steering angle increases, as shown in the contour plots in Figure 4b,c. It can be seen that, as the beam-steering angle increases, new side lobes enter the visible region and, consequently, the SLL increases. Furthermore, the transition to higher SLL depends on the beam width of the entering high-intensity lobe. For antennas with a length of several wavelengths, the secondary lobes present a narrow beam width and the transition between low and high SLLs is relatively abrupt. Therefore, optimizing for large beam-steering ranges prevents the appearance of high-power lobes when the beam is steered within this range. However, this is achieved at the expense of the presence of minor lobes that results in a performance penalty for narrower beam-steering angles.

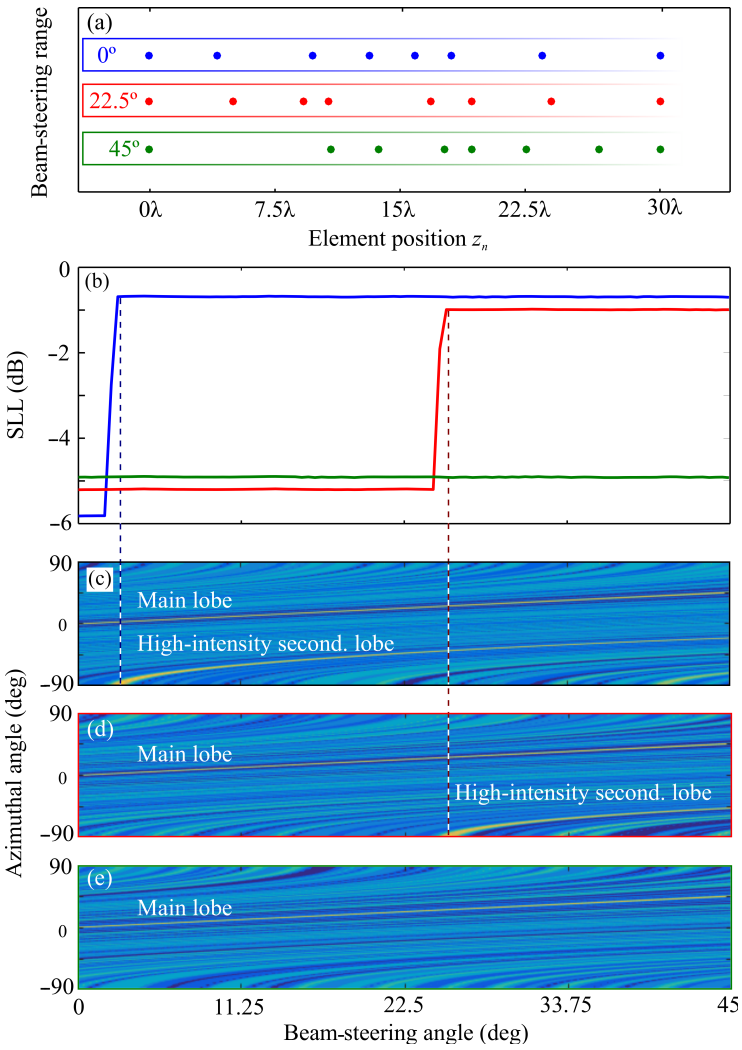

Figure 4. (**a**) Optimized element positions for steering ranges of 0°, 22.5° and 45° for an 8-element array with a minimum separation of 2 λ and a mean distance of 6 λ. (**b**) SLL in terms of the beam-steering angle for the three beam-steering ranges. (**c**–**e**) Modulus of the AF in terms of the beam-steering angle and azimuthal angle θ for the three optimized cases.

We also analyzed the effect of the operation wavelength on the SLL. In Figure 5, we show the SLL in terms of the wavelength for arrays of (a) 4, (b) 8 and (c) 16 elements

optimized for beam-steering angles of 0, 22.5° and 45°. In all cases, the array element positions were optimized for an arbitrary wavelength and then, keeping the positions of the elements constant, the SLL was computed for a wavelength ranging from 0.5 to 1.5 times the design wavelength. As can be seen, when modifying the operation wavelength, the SLL also presents a step-like behavior. In this case, the longer the wavelength is, the lower the SLL. This characteristic shape can be explained using an argument similar to that in Figure 4, but when sweeping the wavelength, instead of a shift of the visible region, the visible region is expanded or compressed. Thus, for a shorter wavelength, the visible region is expanded and some high-intensity lobes that were outside the visible region now enter the visible region. We can then conclude that in terms of the wavelength, the worst-case scenario corresponds to the shortest wavelength.

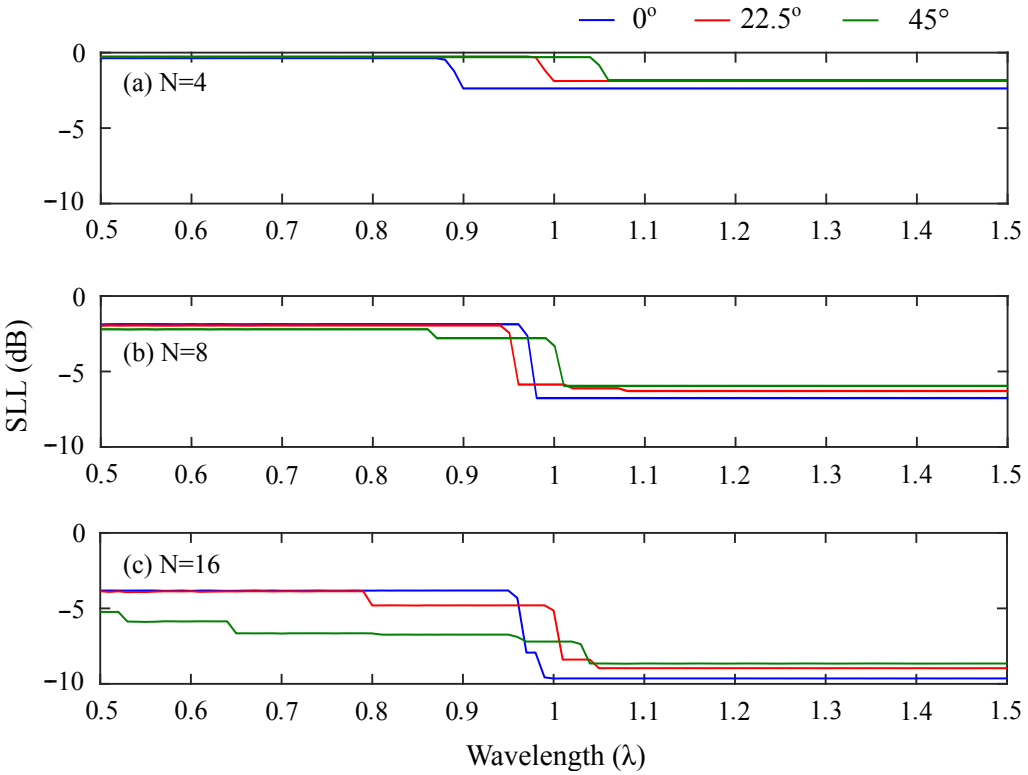

Figure 5. SLL in terms of the operation wavelength for (**a**) 4 elements, (**b**) 8 elements and (**c**) 16 elements. In each case, traces for maximum beam-steering angles of 0°, 22.5° and 45° are presented.

3.2. Effect of the Mean Inter-Element Distance and Beam-Steering Angle on the Side-Lobe Level

One of the most important structural array parameters that affect the SLL of an array is its size, which for the 1D case, is the total length of the array, L. Recalling that the total length can be expressed in terms of the mean inter-element distance, $\bar{d}$ and the number of elements, N, according to $L = N \cdot \bar{d}$, in order to explicitly observe the effect of the mean inter-element distance, $\bar{d}$ was swept. To observe the dependence of the SLL on the mean inter-element distance, in Figure 6, we show the modulus of the AF for three different inter-element values. In addition, to see the effect of the beam-steering angle, the AF for a beam-steering angle of 0°, 22.5° and 45.0° are shown in Figure 6a, Figure 6b and Figure 6c, respectively. As can be seen, independently of the beam-steering angle, both short and long inter-element distances, i.e., 1.1 λ and 5 λ, result in higher values of SLL, whereas an intermediate value of 1.5 λ leads to a better performance in terms of the SLL. An additonal point to note is that, as expected from the results in Section 3.1, the SLL increases as the beam is directed away from the broadside direction.

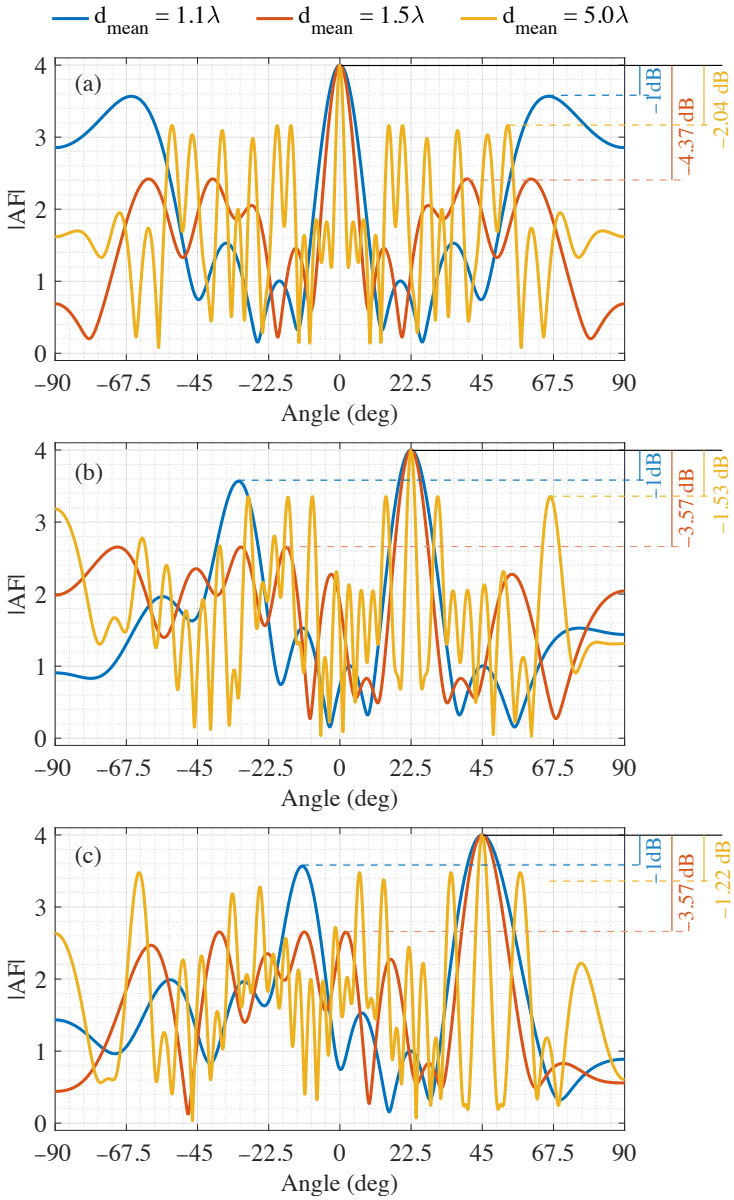

Figure 6. Modulus of the AF for mean inter-element distances of 1.1 λ, 1.5 λ and 5.0 λ for a beam-steering angle of (**a**) 0°, (**b**) 22.5° and (**c**) 45.0°.

3.3. Effect of the Number of Elements and the Average and Minimum Separation on the Side-Lobe Level

Afterward, we proceeded to quantify the SLL in terms of the number of elements as well as the minimum and mean inter-element distance. We considered arrays with 4, 8 and 16 elements and minimum separations of 1 λ, 2 λ and 3 λ. Due to the large number of interacting parameters, in Figure 7 we show different contour plots of the SLL in terms of beam-steering range and mean inter-element distance. Each row corresponds to a number of elements: (a–c) are for 4 radiating elements, (d–f) are for 8 and (g–i) are for 16, whereas each column represents a minimum inter-element distance: (a,d,g) 1 λ, (b,e,h) 2 λ and (c,f,i) 3 λ. Comparing the SLL for different numbers of elements and keeping fixed the minimum inter-element separation, we can see that the larger the element count is, the lower the SLL. On the other hand, if we fixed the number of elements and increase the minimum inter-element distance, a SLL degradation is observed. These results can be interpreted in terms of the trade-off between design freedom and the inherent appearance of side lobes. The degree of freedom can be increased by increasing either the number

of radiating elements or the ratio between the mean distance to the minimum distance. A similar argumentation can be applied to explain why for each configuration, there is a value of mean distance that minimizes the SLL. Thus, if the mean distance is very close to the minimum distance, the design freedom is small and poor SLL is obtained. If the mean separation is too large, the larger freedom in the design cannot compensate for the effect of large element separation. The presence of an optimum mean distance indicates that there is an optimum array length in order to minimize the SLL. This behavior only occurs when physical constraints are introduced and, to our best knowledge, has not been previously reported.

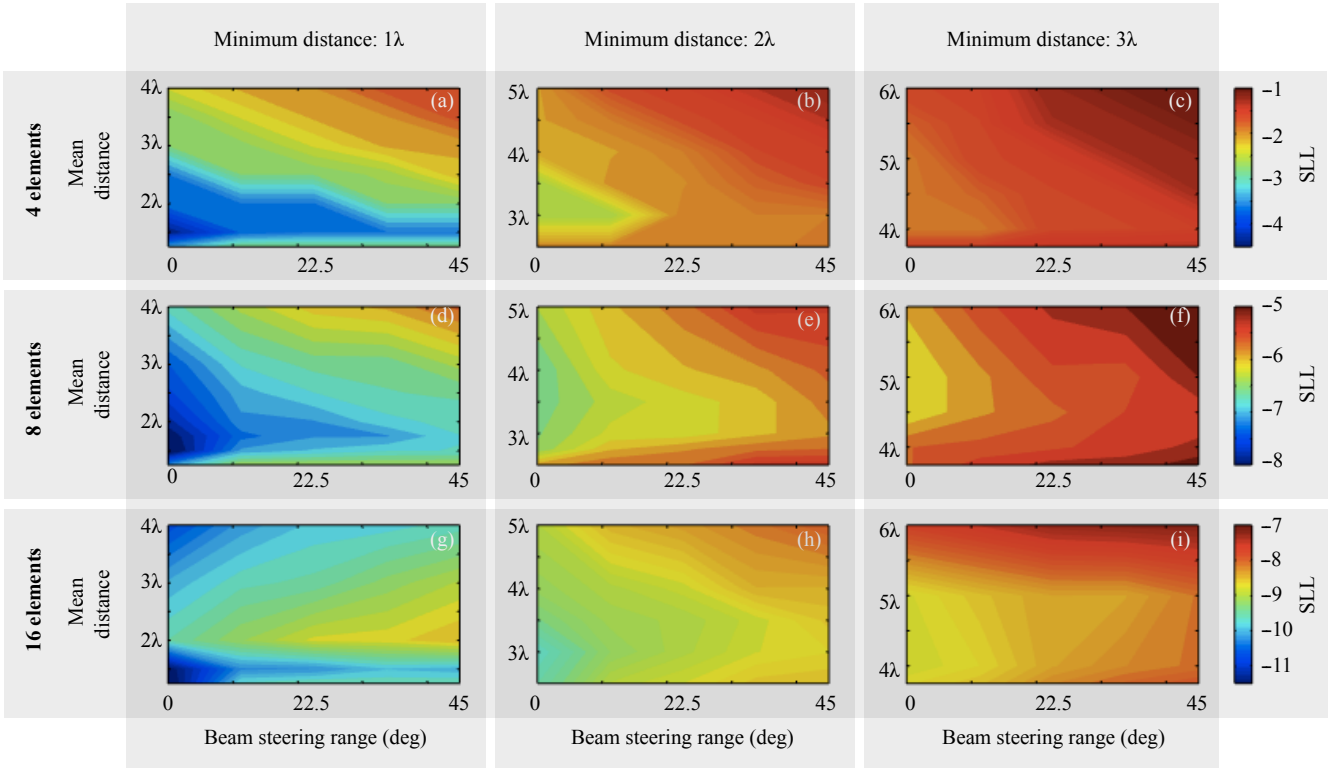

Figure 7. SLL in terms of the mean inter-element distance and beam-steering range for different number of radiating elements and minimum inter-element distance. (**a**–**c**) 4 elements with minimum distances of 1 λ, 2 λ and 3 λ, (**d**–**f**) 8 elements with minimum distances of 1 λ, 2 λ and 3 λ and (**g**–**i**) 16 elements with 1 λ, 2 λ and 3 λ.

The optimum length of a sparse array is an important design parameter, so we analyzed it in more detail. Its dependency on the number of elements, minimum inter-element distance and scanning range is shown in Figure 8a. This optimum mean distance increases with the minimum inter-element separation, whereas it is almost independent of the number of elements and the beam-steering range. Figure 8b shows the SLL values at optimum inter-element spacing for different numbers of elements and minimum separations, revealing that generally speaking, at optimum distance the SLL penalty due to extending the beam-steering range is relatively small. However, for the particular case of a 1 λ separation distance, a significant deterioration of the SLL can be observed for no-null beam-steering ranges. These results have a deep consequence in the design of sectorized arrays. If the initial observation of the dependency of SLL on the beam-steering angle could lead to thinking that sectorization may help in reducing the SLL of the array, when an optimum mean separation is adopted, a marginal SLL reduction can be expected, at least until a four-fold sectorization.

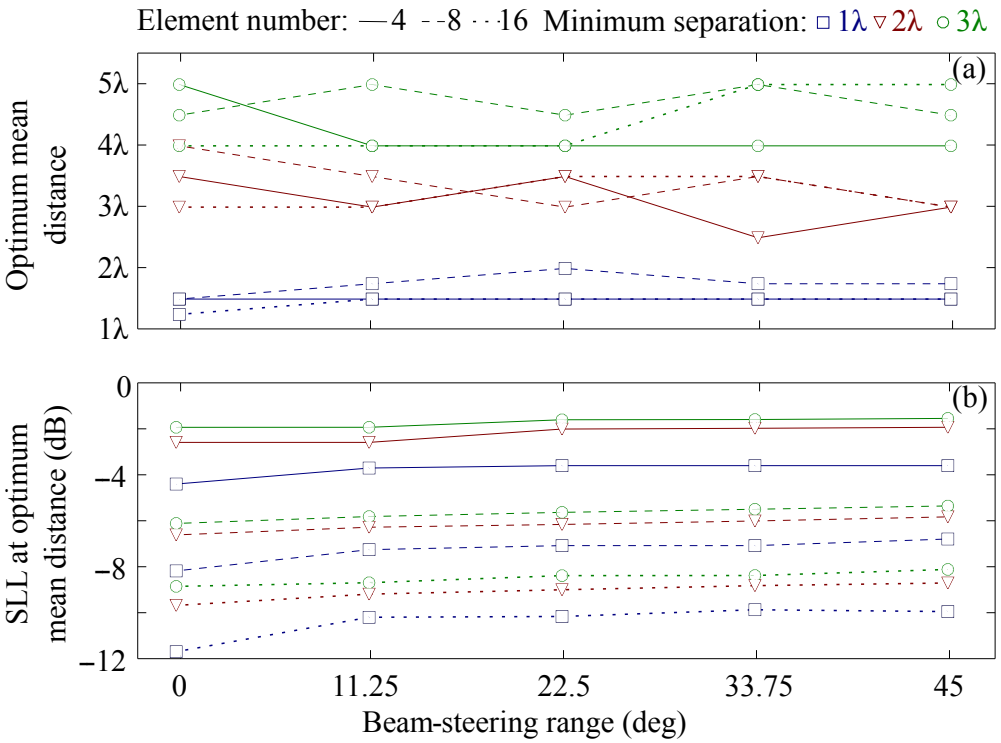

Figure 8. (**a**) Optimum inter-element distance for different numbers of elements and minimum separation. (**b**) SLL at the optimum distance for the different combinations of number of elements and minimum distances.

4. Conclusions

In this paper, we have analyzed the effect of different parameters on the SLL in linear OPAs with a minimum inter-element distance submitted to beam-steering operation. Optimizations of different OPA configurations reveal the following points: (i) The value of SLL increases for broader beam-steering angles and shorter operation wavelength. Therefore, the worst-case scenario corresponds to the extreme value of the field of view and the shortest wavelength of the operation bandwidth. (ii) When a minimum inter-element distance is imposed, there is an optimum mean distance between elements that leads to minimum SLL. This optimum mean distance is particularly sensitive to the minimum inter-element separation while being almost independent of the number of elements and the beam-steering range.

Author Contributions: Conceptualization, I.A., B.D.P.d.S. and R.A.P.; methodology, I.A. and R.A.P.; software, I.A. and B.D.P.d.S.; validation, J.L.P., M.P.d.S. and J.A.d.O.; formal analysis, J.L.P. and M.L.F.A.; resources, I.A. and R.A.P.; data curation, B.D.P.d.S.; writing—original draft preparation, I.A., B.D.P.d.S. and R.A.P.; writing—review and editing, J.L.P., M.P.d.S., M.L.F.A. and J.A.d.O.; visualization, I.A., B.D.P.d.S. and R.A.P.; supervision, I.A. and R.A.P.; project administration, I.A.; funding acquisition, I.A. and R.A.P. All authors have read and agreed to the published version of the manuscript.

Funding: This research was funded by the Sao Paulo State Research Fundation (FAPESP, under grants 15/24517-8 and 18/25339-4) and the National Council for Scientific and Technological Development (CNPq, under grants 311035/2018-3 and 432303/2018-9).

Institutional Review Board Statement: Not applicable.

Informed Consent Statement: Not applicable.

Data Availability Statement: The data presented in this study are available on request from the corresponding author.

Conflicts of Interest: The authors declare no conflict of interest.

Abbreviations

The following abbreviations are used in this manuscript:

LIDAR	Light detection and ranging
OPA	Optical phased array
SLL	Side-lobe level
AF	Array factor
DE	Differential evolution

References

1. Wuytens, P.C.; Skirtach, A.G.; Baets, R. On-chip surface-enhanced Raman spectroscopy using nanosphere-lithography patterned antennas on silicon nitride waveguides. *Opt. Express* **2017**, *25*, 12926–12934. [CrossRef] [PubMed]
2. Poulton, C.V.; Byrd, M.J.; Russo, P.; Timurdogan, E.; Khandaker, M.; Vermeulen, D.; Watts, M.R. Long-range LiDAR and free-space data communication with high-performance optical phased arrays. *IEEE J. Sel. Top. Quantum Electron.* **2019**, *25*, 1–8. [CrossRef]
3. Poulton, C.V.; Yaacobi, A.; Cole, D.B.; Byrd, M.J.; Raval, M.; Vermeulen, D.; Watts, M.R. Coherent solid-state LIDAR with silicon photonic optical phased arrays. *Opt. Lett.* **2017**, *42*, 4091–4094. [CrossRef]
4. Bharadwaj, P.; Deutsch, B.; Novotny, L. Optical antennas. *Adv. Opt. Photonics* **2009**, *1*, 438–483. [CrossRef]
5. Krasnok, A.E.; Miroshnichenko, A.E.; Belov, P.A.; Kivshar, Y.S. All-dielectric optical nanoantennas. *Opt. Express* **2012**, *20*, 20599–20604. [CrossRef] [PubMed]
6. Heck, M.J. Highly integrated optical phased arrays: Photonic integrated circuits for optical beam shaping and beam steering. *Nanophotonics* **2017**, *6*, 93–107. [CrossRef]
7. Michaels, A.; Yablonovitch, E. Reinventing the circuit board with integrated optical interconnects. In Proceedings of the CLEO: Science and Innovations, San Jose, CA, USA, 5–10 June 2016.
8. Sun, X.; Zhang, L.; Zhang, Q.; Zhang, W. Si photonics for practical LiDAR solutions. *Appl. Sci.* **2019**, *9*, 4225. [CrossRef]
9. Pita, J.L.; Aldaya, I.; Santana, O.J.; Dainese, P.; Gabrielli, L.H. Side-lobe level reduction in bio-inspired optical phased-array antennas. *Opt. Express* **2017**, *25*, 30105–30114. [CrossRef]
10. de Souza, B.D.P.; Junior, A.E.F.; Abbade, M.L.F.; Aldaya, I. Side-lobe level reduction in 1D photonic array antennas. In Proceedings of the 2018 SBFoton International Optics and Photonics Conference (SBFoton IOPC), Campinas, Brazil, 8–10 October 2018; pp. 1–4.
11. Barott, W.C.; Steffes, P.G. Grating lobe reduction in aperiodic linear arrays of physically large antennas. *IEEE Antennas Wirel. Propag. Lett.* **2008**, *8*, 406–408. [CrossRef]
12. Phare, C.T.; Shin, M.C.; Sharma, J.; Ahasan, S.; Krishnaswamy, H.; Lipson, M. Silicon Optical Phased Array with Grating Lobe-Free Beam Formation Over 180 Degree Field of View. In Proceedings of the CLEO: Science and Innovations. Optical Society of America, San Jose, CA, USA, 13–18 May 2018.
13. Caratelli, D.; Viganó, M.C. Analytical synthesis technique for linear uniform-amplitude sparse arrays. *Radio Sci.* **2011**, *46*, 1–6. [CrossRef]
14. Suárez, S.; Leon Fernandez, G.; Arrebola, M.; Herrán Ontañón, L.F.; Las Heras Andres, F. Experimental validation of linear aperiodic array for grating lobe suppression. *Prog. Electromagn. Res.* **2012**, *26*, 193–203. [CrossRef]
15. Sandi, E.; Zulkifli, F.Y.; Rahardjo, E.T. A Hybrid Technique Using Combinatorial Cyclic Difference Sets and Binomial Amplitude Tapering for Linear Sparse Array Antenna Design. *Adv. Electromagn.* **2016**, *5*, 73–79. [CrossRef]
16. Trucco, A.; Murino, V. Stochastic optimization of linear sparse arrays. *IEEE J. Ocean. Eng.* **1999**, *24*, 291–299. [CrossRef]
17. Khodier, M.M.; Christodoulou, C.G. Linear array geometry synthesis with minimum sidelobe level and null control using particle swarm optimization. *IEEE Trans. Antennas Propag.* **2005**, *53*, 2674–2679. [CrossRef]
18. Zhang, X.; Zhang, X. Thinning of antenna array via adaptive memetic particle swarm optimization. *EURASIP J. Wirel. Commun. Netw.* **2017**, *2017*, 1–7. [CrossRef]
19. Bray, M.G.; Werner, D.H.; Boeringer, D.W.; Machuga, D.W. Optimization of thinned aperiodic linear phased arrays using genetic algorithms to reduce grating lobes during scanning. *IEEE Trans. Antennas Propag.* **2002**, *50*, 1732–1742. [CrossRef]
20. Hawes, M.B.; Liu, W. Location optimization of robust sparse antenna arrays with physical size constraint. *IEEE Antennas Wirel. Propag. Lett.* **2012**, *11*, 1303–1306. [CrossRef]
21. Hawes, M.B.; Liu, W. Sparse microphone array design for wideband beamforming. In Proceedings of the 2013 18th International Conference on Digital Signal Processing (DSP), Fira, Greece, 1–3 July 2013; pp. 1–5.
22. Hawes, M.B.; Liu, W. Compressive sensing-based approach to the design of linear robust sparse antenna arrays with physical size constraint. *IET Microw. Antennas Propag.* **2014**, *8*, 736–746. [CrossRef]
23. Raji, M.F.; Zhao, H.; Monday, H.N. Fast optimization of sparse antenna array using numerical Green's function and genetic algorithm. *Int. J. Numer. Model. Electron. Netw. Devices Fields* **2019**, *33*, e2544. [CrossRef]
24. Li, M.; Wei, H.; Zhao, J.; Tao, Q.; You, Z. A Novel Linear Sparse Array with Reconfigurable Pixel Antenna Elements. *Int. J. Antennas Propag.* **2020**, *2020*, 3624563. [CrossRef]
25. Dib, N.I.; Goudos, S.K.; Muhsen, H. Application of Taguchi's optimization method and self-adaptive differential evolution to the synthesis of linear antenna arrays. *Prog. Electromagn. Res.* **2010**, *102*, 159–180. [CrossRef]

26. Zhang, F.; Jia, W.; Yao, M. Linear aperiodic array synthesis using differential evolution algorithm. *IEEE Antennas Wirel. Propag. Lett.* **2013**, *12*, 797–800. [CrossRef]
27. Wang, R.Q.; Jiao, Y.C.; Zhang, H.; Zhou, Z. Synthesis of unequally spaced linear arrays using modified differential evolution algorithm. *IET Microw. Antennas Propag.* **2018**, *12*, 1908–1912. [CrossRef]
28. Coman, C.I.; Lager, I.E.; Ligthart, L.P. Design considerations in sparse array antennas. In Proceedings of the European Radar Conference, Manchester, UK, 13–15 September 2006; pp. 72–75.
29. Zhang, D.; Zhang, F.; Pan, S. Grating-lobe-suppressed optical phased array with optimized element distribution. *Opt. Commun.* **2018**, *419*, 47–52. [CrossRef]
30. Liu, Q.; Lu, Y.; Wu, B.; Jiang, P.; Cao, R.; Feng, J.; Guo, J.; Jin, L. Silicon Optical Phased Array Side Lobe Suppression Based on an Improved Genetic Algorithm. In Proceedings of the 2020 Asia Communications and Photonics Conference (ACP) and International Conference on Information Photonics and Optical Communications (IPOC), Beijing, China, 24–27 October 2020; pp. 1–3.
31. Du, K.; Wang, R.; Guo, J.; Jiang, R.; Kan, D.; Zhang, Y. Design of a sparse array for a one-dimensional non-uniform optical phased array. *JOSA B* **2022**, *39*, 1141–1146. [CrossRef]
32. Storn, R.; Price, K. Differential evolution—A simple and efficient heuristic for global optimization over continuous spaces. *J. Glob. Optim.* **1997**, *11*, 341–359. [CrossRef]
33. Qing, A.; Lee, C.K. *Differential Evolution in Electromagnetics*; Springer: Heidelberg/Berlin, Germany, 2010.